SAE 86B20
Quenched Core (ATM)
Iteration #74

Microstructural Data, Monotonic
And
Fatigue Test Results

Prepared by:

F. Yin
and
A. Fatemi

Department of Mechanical, Industrial and
Manufacturing Engineering
The University of Toledo
Toledo, Ohio 43606

Prepared for:
The AISI Bar Steel Applications Group

April 2005

TABLE OF CONTENTS

NOMENCLATURE

A_o, A_f	initial, final area	S	engineering stress
HB, HRB, HRC	Brinell, Rockwell B-Scale, Rockwell C-Scale hardness number	YS, UYS, LYS, YS'	monotonic yield, upper yield, lower yield, cyclic yield strength
b, c, n	fatigue strength, fatigue ductility, strain hardening exponent	YPE	yield point elongation
D_o, D_f	initial, final diameter	S_u	ultimate tensile strength
e	engineering strain	%EL	percent elongation
E, E'	monotonic, midlife cycle modulus of elasticity	%RA	percent reduction in area
K, K'	monotonic, cyclic strength coefficient	σ, σ_f, σ_f'	true stress, true fracture strength, fatigue strength coefficient
L_o, L_f	initial, final gage length	σ_a, σ_m, $\Delta\sigma$	stress amplitude, mean stress, stress range
$N_{50\%}$, $(N_f)_{10\%}$, $(N_f)_{50\%}$	number of cycles to midlife, 10% load drop, 50% load drop	ε_e, ε_p, ε	true elastic, plastic, total strain
$2N_f$	reversals to failure	ε_f, ε_f'	true fracture ductility, fatigue ductility coefficient
P_f, P_u	fracture, ultimate load	ε_a, ε_m, $\Delta\varepsilon$	strain amplitude, mean strain, strain range
R	neck radius; or strain ratio	$\Delta\varepsilon_e$, $\Delta\varepsilon_p$	elastic, plastic strain range

UNIT CONVERSION TABLE

Measure	SI Unit	US Unit	from SI to US	from US to SI
Length	mm	in	$1 \text{ mm} = 0.03937 \text{ in}$	$1 \text{ in} = 25.4 \text{ mm}$
Area	mm^2	in^2	$1 \text{ mm}^2 = 0.00155 \text{ in}^2$	$1 \text{ in}^2 = 645.16 \text{ mm}^2$
Load	kN	klb	$1 kN = 0.2248 \text{ klb}$	$1 \text{ klb} = 4.448 \text{ kN}$
Stress	MPa	ksi	$1 \text{ MPa} = 0.14503 \text{ ksi}$	$1 \text{ ksi} = 6.895 \text{ MPa}$
Temperature	^{o}C	^{o}F	$^{o}C = (^{o}F - 32)/1.8$	$^{o}F = (^{o}C * 1.8) + 32$

In SI Unit:

$1 \text{ kN} = 10^3 \text{ N}$ $1 \text{ Pa} = 1 \text{ N/m}^2$ $1 \text{ MPa} = 10^6 \text{ Pa} = 1 \text{ N/mm}^2$ $1 \text{ Gpa} = 10^9 \text{ Pa}$

In US Unit:

$1 \text{ klb} = 10^3 \text{ lb}$ $1 \text{ psi} = 1 \text{ lb/in}^2$ $1 \text{ ksi} = 10^3 \text{ psi}$

SUMMARY

The microstructural data, monotonic properties, and fatigue behavior data have been obtained for SAE 86B20 Quenched Core (Atm) steel. The material was provided by the American Iron and Steel Institute (AISI). Microstructural data includes grain type, grain size, and inclusion content. Two tensile tests were performed to acquire the desired monotonic properties. Eighteen strain-controlled fatigue tests were performed to obtain the strain-life and cyclic stress-strain curves and properties. The experimental procedure followed and results obtained are presented and discussed in this report.

I. EXPERIMENTAL PROGRAM

1.1 Material and Specimen Fabrication

1.1.1 Material

The SAE 86B20 Quenched Core (Atm) steel was manufactured by MacSteel Company. This material was delivered to the University of Toledo in circular bar form. The bars were approximately 2.111 inch in diameter prior to machining. In Table 1, the chemical composition supplied by AISI is shown.

1.1.2 Specimen

In this study, identical round specimens were used for the monotonic and fatigue tests. The specimen configuration and dimensions are shown in Figure 1. This configuration deviates slightly from the specimens recommended by ASTM Standard E606 [1]. The recommended specimens have uniform or hourglass test sections. The specimen geometry shown in Figure 1 differs by using a large secondary radius throughout the test section.

All specimens were machined in the Mechanical, Industrial, and Manufacturing Engineering Machine Shop at the University of Toledo. The specimens were initially waterjet-cut at Ford Motor Company to an appropriate diameter and length for insertion into a CNC machine. Using the CNC machine, final turning was performed to achieve the tolerable dimensions specified on the specimen drawings. Then the specimens were polished.

A commercial round-specimen polishing machine was used to polish the specimen gage section. Four different grits of aluminum oxide lapping film were used: 30μ, 15μ, 9μ, and 3μ. The 3μ grit was used as the final polish and polishing marks coincided with the specimens' longitudinal direction. The polished surfaces were carefully examined under magnification to ensure complete removal of machine marks within the test section. After Polishing, specimens were heat treated and tested.

1.2 Testing Equipment

1.2.1 Apparatus

An INSTRON 8801 closed-loop servo-hydraulic axial load frame in conjunction with a Fast-Track digital servo-controller was used to conduct the tests. The calibration of this system was verified prior to beginning the test program. The load cell used had a capacity of 11 klb. Hydraulically operated grips using universal tapered collets were employed to secure the specimens' ends in series with the load cell.

Total strain was controlled for all tests using an extensometer rated as ASTM class B1 [2]. The calibration of the extensometer was verified using displacement apparatus containing a micrometer barrel in divisions of 0.0001 in. The extensometer had a gage length of 0.30 in and was capable of measuring strains up to 15 %.

In order to protect the specimens' surface from the knife-edges of the extensometer, ASTM Standard E606 recommends the use of transparent tape or epoxy to 'cushion' the attachment. For this study, it was found that application of transparent tape strips was difficult due to the radius within the test section. Therefore, epoxy was

considered to be the best protection. One disadvantage of epoxy is the variability of mixtures throughout the test program. As an alternative to epoxy, M-coat D offered a more consistent mixture. Therefore, the tests were performed using M-coat D.

1.2.2 Alignment

Significant effort was put forth to align the load train (load cell, grips, specimen, and actuator). Misalignment can result from both tilt and offset between the central lines of the load train components. According to ASTM Standard E606, the maximum bending strains should not exceed 5 % of the minimum axial strain range imposed during any test program. For this study, the minimum axial strain range was 0.0045 in/in. Therefore, the maximum allowable bending strain was 225 microstrain. ASTM Standard E1012, Type A, Method 1 was followed to verify specimen alignment [3]. For this procedure, two arrays of four strain gages per array were arranged at the upper and lower ends of the uniform gage section. For each array, gages were equally spaced around the circumference of a 0.5-in. uniform diameter bar. The maximum bending strain determined from the gaged specimen was less than 60 microstrain. This value was well within the allowable ASTM limit.

1.3 Test Methods and Procedures

1.3.1 Monotonic tension tests

All monotonic tests in this study were performed using test methods specified by ASTM Standard E8 [4]. Two specimens were used to obtain the monotonic properties.

1.3 Test Methods and Procedures

1.3.1 Monotonic tension tests

All monotonic tests in this study were performed using test methods specified by ASTM Standard E8 [4]. Two specimens were used to obtain the monotonic properties. Due to the limitations of the extensometer, strain control was used only up to 14% strain. After this point, displacement control was used until fracture.

For the elastic and initial yield region (0% to 0.5% strain), a strain rate of 0.0025 in/in/min was chosen. This strain rate was three-quarters of the maximum allowable rate specified by ASTM Standard E8 for the initial yield region. After yielding (0.5% to 14% strain), the strain rate was increased by a factor of three (i.e., 0.0075 in/in/min). After the extensometer was removed, a displacement rate of 0.01275 in/min was used. This displacement rate provided approximately the same strain rate as that used prior to switching control modes.

After the tension tests were concluded, the broken specimens were carefully reassembled. The final gage lengths of the fractured specimens were measured with a Vernier caliper having divisions of 0.001 in. Using an optical comparator with 10X magnification and divisions of 0.001 in, the final diameter and the neck radius were measured. It should be noted that prior to the test, the initial minimum diameter was measured with this same instrument.

1.3.2 Constant amplitude fatigue tests

All constant amplitude fatigue tests in this study were performed according to ASTM Standard E606. It is recommended by this standard that at least 10 specimens be

used to generate the fatigue properties. For this study, 18 specimens at 7 different strain amplitudes ranging from 0.225% to 2% were utilized. INSTRON LCF software was used in all the strain-controlled tests. During each strain-controlled test, the total strain was recorded using the extensometer output. Test data were automatically recorded throughout each test.

There were two control modes used for these tests. Strain control was used in all tests with plastic deformation. For all the elastic tests (except for one of the run-out tests which was conducted in load control throughout), strain control was used initially to determine the stabilized load, then load control was used for the remainder of the test. The reason for the change in control mode was due to limitations on the extensometer for high test frequencies. For the strain control tests, the applied frequencies ranged from 0.2 Hz to 2 Hz in order to keep a strain rate about 0.02 in/in/sec. For the load control tests, the frequency was increased to 10 to 25 Hz in order to shorten the overall test duration. All strain-controlled tests were conducted using a triangular waveform and all load-controlled tests were conducted using a Sine waveform.

II. EXPERIMENTAL RESULTS AND ANALYSIS

2.1 Microstructure Data

Photomicrographs of the microstructure were obtained using an optical microscope with a digital camera attachment. It was observed that the grains in the transverse and longitudinal directions had negligible difference. In Figure 2a and 2b, the microstructure pictures in the longitudinal (L-T) direction and the transverse (T'-T) direction are shown at 500X magnification respectively. It can be seen from these photomicrographs that SAE 86B20 Quenched Core (Atm) steel had a ferritic-pearlitic microstructure both in L-T direction and T'-T direction. In Figure 3a and 3b, the inclusions/voids in L-T and T'-T directions are shown at 100X magnification. For Figures 2a and 3a, the rolling direction is parallel to the page, and for Figures 2b and 3b, the rolling direction is perpendicular to the page.

The average grain size was measured in both transverse and longitudinal directions using the comparison procedure reported in ASTM Standard E112 [5]. According to ASTM Standard E45, method A, the inclusion rating numbers for type D inclusion in both L-T and T'-T directions were found [6]. Rockwell hardness test was also performed. A summary of the microstructure data for SAE 86B20 Quenched Core (Atm) steel is provided in Table 2.

2.2 Monotonic Deformation Behavior

The properties determined from monotonic tests were the following: modulus of elasticity (E), yield strength (YS), upper yield strength (UYS), lower yield strength (LYS), yield point elongation (YPE), ultimate tensile strength (S_u), percent elongation (%EL), percent reduction in area (%RA), true fracture strength (σ_f), true fracture ductility (ε_f), strength coefficient (K), and strain hardening exponent (n).

True stress (σ), true strain (ε), and true plastic strain (ε_p) were calculated from engineering stress (S) and engineering strain (e), according to the following relationships which are based on constant volume assumption:

$$\sigma = S(1 + e) \tag{1a}$$

$$\varepsilon = \ln(1 + e) \tag{1b}$$

$$\varepsilon_p = \varepsilon - \varepsilon_e = \varepsilon - \frac{\sigma}{E} \tag{1c}$$

The true stress (σ) - true strain (ε) plot is often represented by the Ramberg-Osgood equation:

$$\varepsilon = \varepsilon_e + \varepsilon_p = \frac{\sigma}{E} + \left(\frac{\sigma}{K}\right)^{\frac{1}{n}} \tag{2}$$

The strength coefficient, K, and strain hardening exponent, n, are the intercept and slope of the best line fit to true stress (σ) versus true plastic strain (ε_p) data in log-log scale:

$$\sigma = K\left(\varepsilon_p\right)^n \tag{3}$$

In accordance with ASTM Standard E739 [7], when performing the least squares fit, the true plastic strain (ε_p) was the independent variable and the stress (σ) was the dependent variable. These plots for the two tests conducted are shown in Figure 4. To generate the K and n values, the range of data used in this figure was chosen according to the definition of discontinuous yielding specified in ASTM Standard E646 [8]. Therefore, the valid data range occurred between the end of yield point extension and the strain at or prior to maximum load.

The true fracture strength, σ_f, was corrected for necking according to the Bridgman correction factor [10]:

$$\sigma_f = \frac{\dfrac{P_f}{A_f}}{\left(1 + \dfrac{4R}{D_f}\right) \ln\left(1 + \dfrac{D_f}{4R}\right)} \tag{4}$$

where P_f is the load at fracture, R is the neck radius, and D_f is the diameter at fracture.

The true fracture ductility, ε_f, was calculated from the relationship based on constant volume:

$$\varepsilon_f = \ln\left(\frac{A_o}{A_f}\right) = \ln\left(\frac{1}{1 - RA}\right) \tag{5}$$

where A_f is the cross-sectional area at fracture, A_o is the original cross-sectional area, and RA is the reduction in area.

A summary of the monotonic properties for SAE 86B20 Quenched Core (Atm) steel is provided in Table 2. The monotonic stress-strain curves are shown in Figure 5. As

can be seen from this figure, the two curves are considerably close to each other. Refer to Table A.1 in the Appendix for a summary of the monotonic test results.

2.3 Cyclic Deformation Behavior

2.3.1 Transient cyclic response

Transient cyclic response describes the process of cyclic-induced change in deformation resistance of a material. Data obtained from constant amplitude strain-controlled fatigue tests were used to determine this response. Plots of stress amplitude variation versus applied number of cycles can indicate the degree of transient cyclic softening/hardening. Also, these plots show when cyclic stabilization occurs. A composite plot of the transient cyclic response for SAE 86B20 Quenched Core (Atm) steel is shown in Figure A.1 of the Appendix. The transient response was normalized on the rectangular plot in Figure A.1a, while a semi-log plot is shown in Figure A.1b. Even though multiple tests were conducted at each strain amplitude, data from one test at each strain amplitude tested are shown in these plots.

2.3.2 Steady-state cyclic deformation

Another cyclic behavior of interest was the steady state or stable response. Data obtained from constant amplitude strain-controlled fatigue tests were also used to determine this response. The properties determined from the steady-state hysteresis loops were the following: cyclic modulus of elasticity (E'), cyclic strength coefficient (K'),

cyclic strain hardening exponent (n'), and cyclic yield strength (YS'). Half-life (midlife) hysteresis loops and data were used to obtain the stable cyclic properties.

Similar to monotonic behavior, the cyclic true stress-strain behavior can be characterized by the Ramberg-Osgood type equation:

$$\frac{\Delta \varepsilon}{2} = \frac{\Delta \varepsilon_e}{2} + \frac{\Delta \varepsilon_p}{2} = \frac{\Delta \sigma}{2E} + \left(\frac{\Delta \sigma}{2K'}\right)^{\frac{1}{n'}} \tag{6}$$

It should be noted that in Equation 6 and the other equations that follow, E is the average modulus of elasticity that was calculated from the monotonic tests.

The cyclic strength coefficient, K', and cyclic strain hardening exponent, n', are the intercept and slope of the best line fit to true stress amplitude ($\Delta\sigma/2$) versus true plastic strain amplitude ($\Delta\varepsilon_p/2$) data in log-log scale:

$$\frac{\Delta \sigma}{2} = K'\left(\frac{\Delta \varepsilon_p}{2}\right)^{n'} \tag{7}$$

In accordance with ASTM Standard E739, when performing the least squares fit, the true plastic strain amplitude ($\Delta\varepsilon_p/2$) was the independent variable and the stress amplitude ($\Delta\sigma/2$) was the dependent variable. The true plastic strain amplitude was calculated by the following equation:

$$\frac{\Delta \varepsilon_p}{2} = \frac{\Delta \varepsilon}{2} - \frac{\Delta \sigma}{2E} \tag{8}$$

This plot is shown in Figure 6. To generate the K' and n' values, the range of data used in the figure was chosen for $[\Delta\varepsilon_p/2]$ calculated ≥ 0.0010 in/in.

The cyclic stress - strain curve reflects the resistance of a material to cyclic deformation and can be vastly different from the monotonic stress - strain curve. The

11

cyclic stress - strain curve is shown in Figure 7. In Figure 8, superimposed plots of monotonic and cyclic curves are shown. As can be seen in Figure 8, SAE 86B20 Quenched Core (Atm) steel cyclically softens. Figure A.2 in the Appendix shows a composite plot of the steady-state (midlife) hysteresis loops. Even though multiple tests were conducted at each strain amplitude, the stable loops from only one test at each strain amplitude are shown in this plot.

2.4 Constant Amplitude Fatigue Behavior

Constant amplitude strain-controlled fatigue tests were performed to determine the strain-life curve. The following equation relates the true strain amplitude to the fatigue life:

$$\frac{\Delta \varepsilon}{2} = \frac{\Delta \varepsilon_e}{2} + \frac{\Delta \varepsilon_p}{2} = \frac{\sigma_f'}{E}\left(2N_f\right)^b + \varepsilon_f'\left(2N_f\right)^c \qquad (9)$$

where σ_f' is the fatigue strength coefficient, b is the fatigue strength exponent, ε_f' is the fatigue ductility coefficient, c is the fatigue ductility exponent, E is the monotonic modulus of elasticity, and $2N_f$ is the number of reversals to failure (which was defined as a 50% load drop, as recommended by ASTM Standard E606).

The fatigue strength coefficient, σ_f', and fatigue strength exponent, b, are the intercept and slope of the best line fit to true stress amplitude ($\Delta\sigma/2$) versus reversals to failure ($2N_f$) data in log-log scale:

$$\frac{\Delta \sigma}{2} = \sigma_f'\left(2N_f\right)^b \qquad (10)$$

In accordance with ASTM Standard E739, when performing the least squares fit, the stress amplitude ($\Delta\sigma/2$) was the independent variable and the reversals to failure ($2N_f$) was the dependent variable. This plot is shown in Figure 9. To generate the σ_f' and b values, the range of data used in this figure was chosen for $N_f \le 10^6$ cycles.

The fatigue ductility coefficient, ε_f', and fatigue ductility exponent, c, are the intercept and slope of the best line fit to calculated true plastic strain amplitude ($\Delta\varepsilon_p/2$) versus reversals to failure ($2N_f$) data in log-log scale:

$$\left(\frac{\Delta\varepsilon_p}{2}\right)_{calculated} = \varepsilon_f' \left(2N_f\right)^C \tag{11}$$

In accordance with ASTM Standard E739, when performing the least squares fit, the calculated true plastic strain amplitude ($\Delta\varepsilon_p/2$) was the independent variable and the reversals to failure ($2N_f$) was the dependent variable. The calculated true plastic strain amplitude was determined from Equation 8. This plot is shown in Figure 10. To generate the ε_f' and c values, the range of data used in this figure was chosen for $[\Delta\varepsilon_p/2]_{calculated} \ge 0.0010$ in/in.

The true strain amplitude versus reversals to failure plot is shown in Figure 11. This plot displays the strain - life curve (Eqn. 9), the elastic strain portion (Eqn. 10), the plastic strain portion (Eqn. 11), and superimposed fatigue data. A summary of the cyclic properties for SAE 86B20 Quenched Core (Atm) steel is provided in Table 2. Table A.2 in the Appendix provides the summary of the fatigue test results.

Table 1: Chemical composition of SAE 86B20 Quenched Core (Atm) steel

Element	Wt. %
Carbon, C	0.19%
Manganese, Mn	0.90%
Phosphorus, P	0.018%
Sulfur, S	0.029%
Silicon, Si	0.240%
Nickel, Ni	0.36%
Chromium, Cr	0.58%
Molybdenum, Mo	0.20%
Copper, Cu	0.24%
Tin, Sn	0.009%
Aluminum, Al	0.021%
Titanium, Ti	0.034%
Boron, B	0.0020%
Calcium, Ca	0.0008%
Nitrogen, N	0.0065%

Table 2: Summary of the Mechanical Properties

Microstructural Data	Average
ASTM grain size number (MAG=500X):	
Transverse direction (T-T')	7 to 8
Longitudinal direction (L-T)	7 to 8
Inclusion rating number (MAG=100X):	
Type A (sulfide type), thin series	none
Type B (alumina type), thin series	none
Type C (silicate type), thin series	none
Type D (globular type), thin series	L-T: 3.5, thin; T'-T: 2.5, thin
Hardness:	
Brinell (HB)	
Transverse direction (T-T')	NA
Longitudinal direction (L-T)	NA
Rockwell B-scale (HRB)	
Transverse direction (T-T')	108.9
Longitudinal direction (L-T)	109.5
Rockwell C-scale (HRC)	
Transverse direction (T-T')	35.8
Longitudinal direction (L-T)	36.0
Microstructure type:	
Transverse direction (T-T')	ferrite/pearlite
Longitudinal direction (L-T)	ferrite/pearlite

Monotonic Properties	Average		Range	
Modulus of elasticity, E, GPa (ksi):	204.5	(29,655.9)	203.8 - 205.1	(29,564.0 - 29,747.7)
Yield strength (0.2% offset), YS , MPa (ksi):	989.0	(143.4)	982.5 - 995.6	(142.5 - 144.4)
Upper yield strength UYS, MPa (ksi):	995.9	(144.4)		
Lower yield strength LYS, MPa (ksi):	980.1	(142.2)		
Yield point elongation, YPE (%):	0.70%			
Ultimate strength, S_u , MPa (ksi):	1034.1	(150.0)	1027.4 - 1040.8	(149.0 - 150.9)
Percent elongation, %EL (%):	29.7%		29.3% - 30.0%	
Percent reduction in area, %RA (%):	63.7%		63.6% - 63.8%	
Strength coefficient, K , MPa (ksi):	1,213.0	(175.9)	1,208.5 - 1,217.5	(175.3 - 176.6)
Strain hardening exponent, n:	0.0369		0.0358 - 0.0379	
True fracture strength, σ_f *, MPa (ksi):	869.0	(126.0)	858.8 - 879.2	(124.6 - 127.5)
True fracture ductility, ε_f (%):	101.3%		101.1% - 101.5%	

Cyclic Properties	Average		Range	
Cyclic modulus of elasticity, E' , GPa (ksi):	192.9	(27,983.1)	170.1 - 209.3	(24,676.2 - 30,349.0)
Fatigue strength coefficient, σ_f' , MPa (ksi):	1,284.1	(186.2)		
Fatigue strength exponent, b:	-0.0652			
Fatigue ductility coefficient, ε_f' :	1.3467			
Fatigue ductility exponent, c:	-0.7256			
Cyclic yield strength, YS', MPa (ksi)	705.4	(102.3)		
Cyclic strength coefficient, K' , MPa (ksi):	1,267.6	(183.8)		
Cyclic strain hardening exponent, n':	0.0943			
Fatigue strength @ 10^6 cycles, S_f, Mpa (ksi)	498.6	(72.3)		

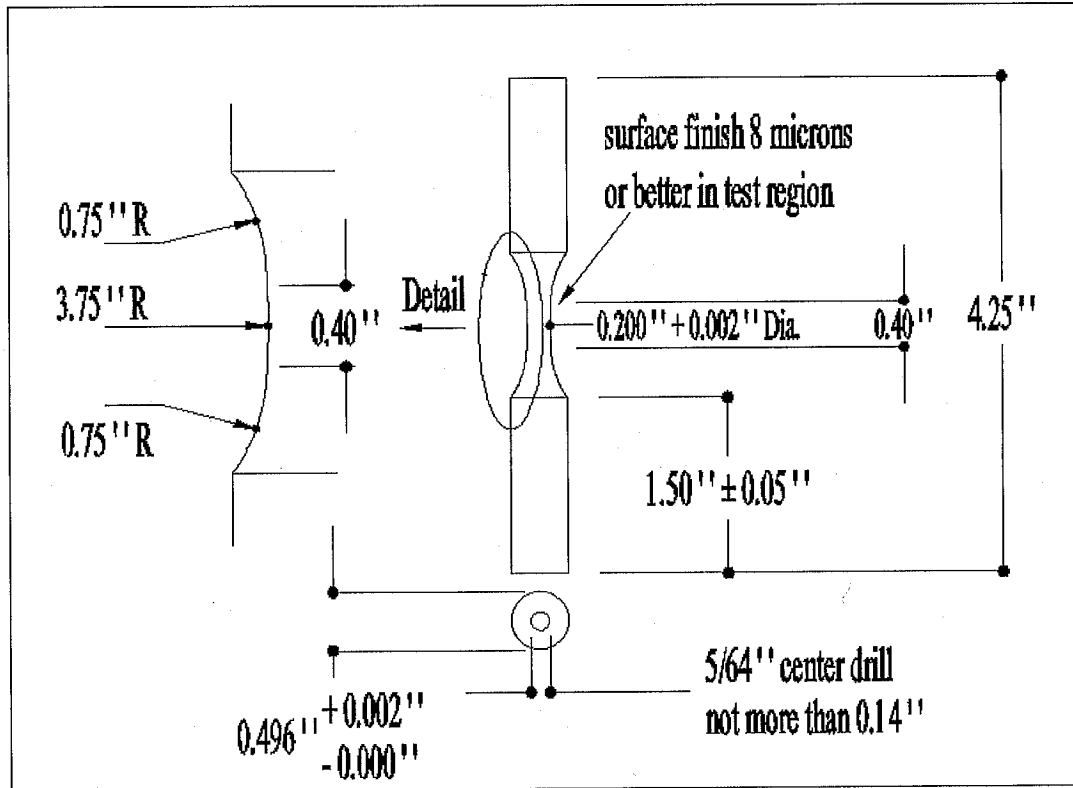* Correction was made according to the Bridgman correction factor.
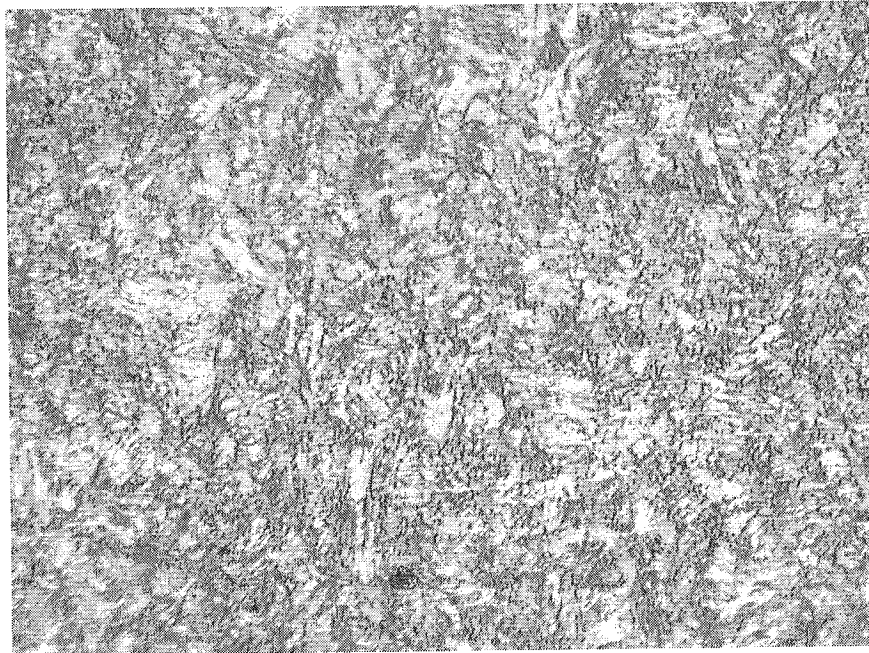
Figure 1: Specimen configuration and dimensions

Figure 2a: Photomicrograph in longitudinal direction (L-T) at 500X
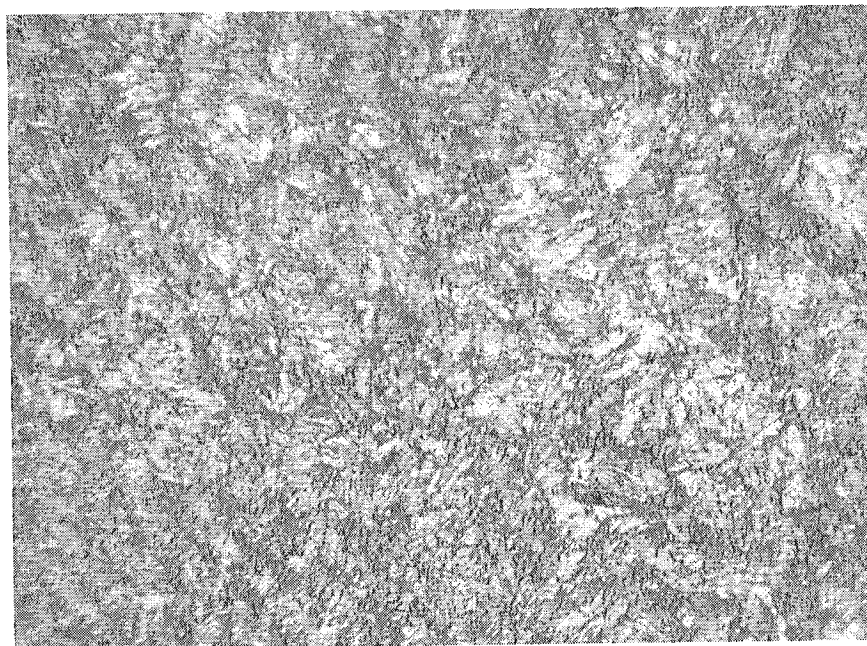for SAE 86B20 Quenched Core (Atm) steel (rolling direction is parallel to the page).

Figure 2b: Photomicrograph in transverse direction (T'-T) at 500X
for 86B20 Quenched Core (Atm) steel (rolling direction is perpendicular to the page).
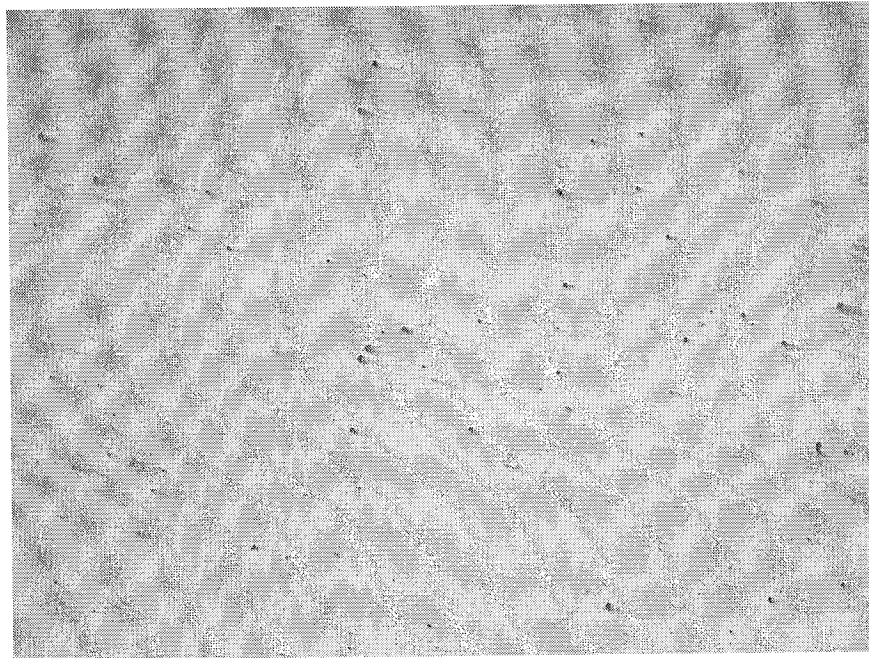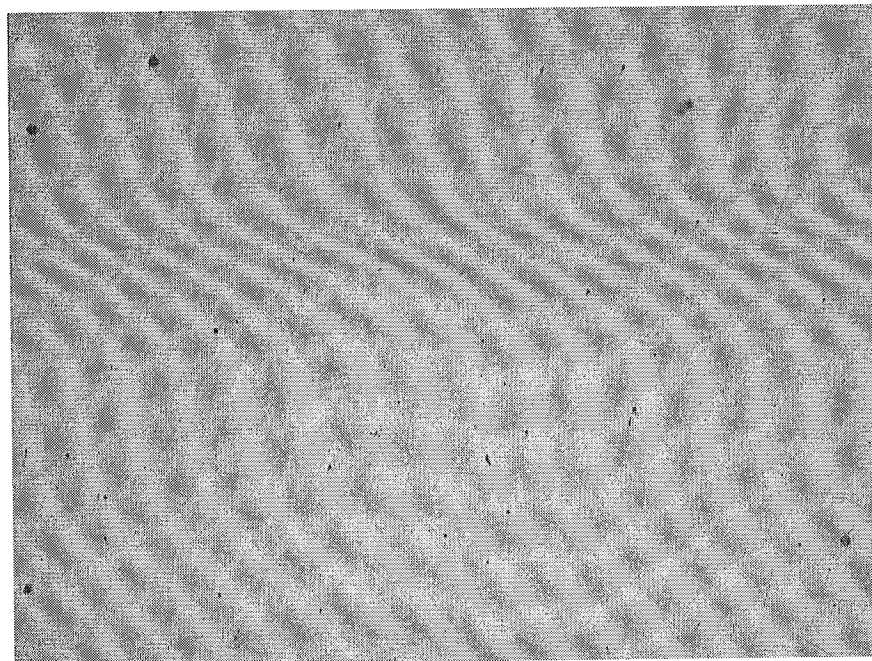
Figure 3a: Examples of inclusions in the longitudinal direction (L-T) at 100X
for SAE 86B20 Quenched Core (Atm) steel (rolling direction is parallel to the page).
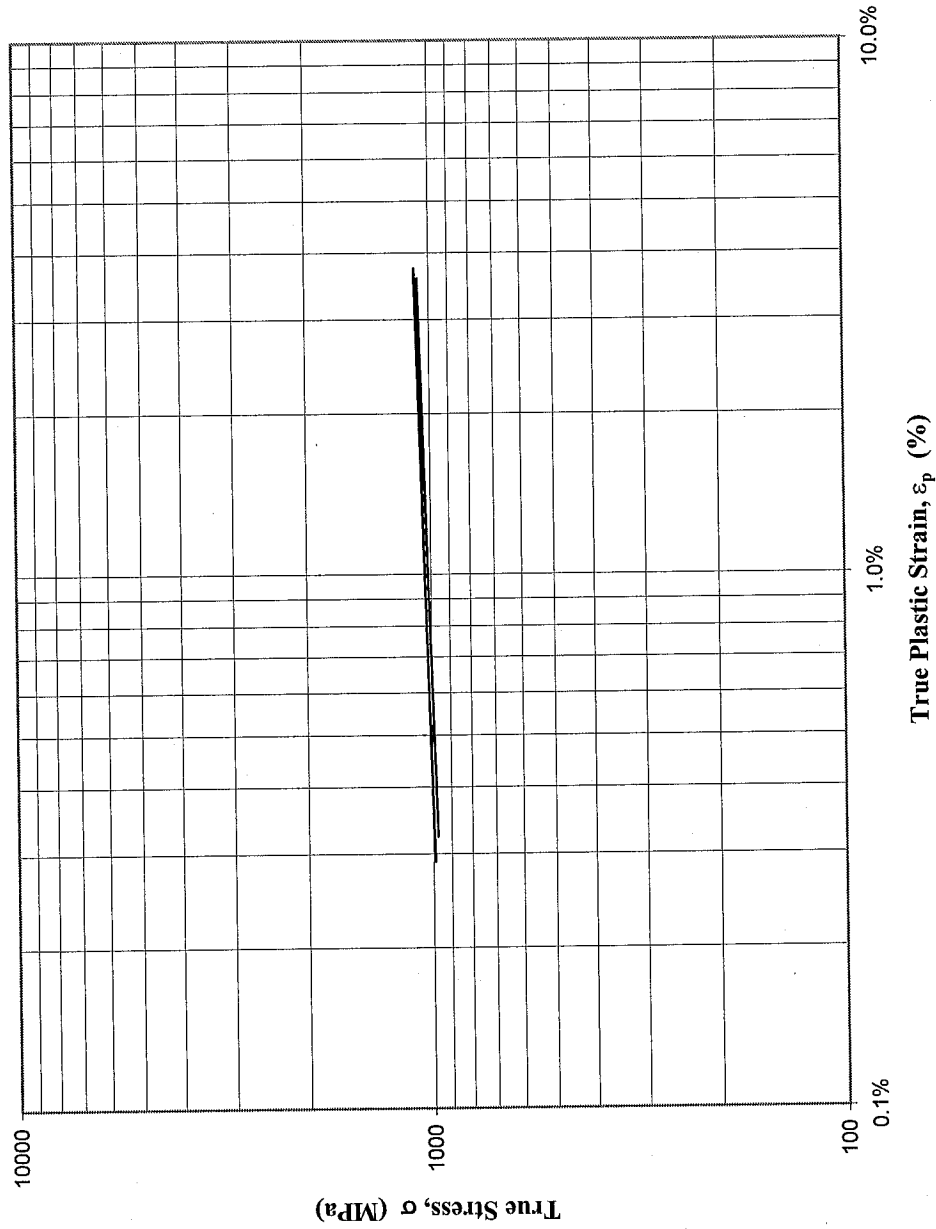

Figure 3b: Examples of inclusions in the transverse direction (T'-T) at 100X
for SAE 86B20 Quenched Core (Atm) steel (rolling direction is perpendicular to the page).

True Stress vs. True Plastic Strain

G1-3:
$\sigma = 1217.5 \, (\varepsilon_p)^{0.0358}$
$K = 1217.5$ MPa
$n = 0.0358$
$R^2 = 0.9653$

G1-2:
$\sigma = 1208.5 \, (\varepsilon_p)^{0.0379}$
$K = 1208.5$ MPa
$n = 0.0379$
$R^2 = 0.9588$

Specimen ID:
(top to bottom)
G1-3
G1-2

True Plastic Strain, ε_p (%)

True Stress, σ (MPa)

Figure 4: True stress versus true plastic strain

19

Figure 5: Monotonic stress-strain curve

True Stress Amplitude vs. True Plastic Strain Amplitude (Calculated)

$$\Delta\sigma/2 = 1267.6 \, (\Delta\varepsilon_p/2)^{0.0943}$$
$$K' = 1267.6 \text{ MPa}$$
$$n' = 0.0943$$
$$R^2 = 0.9764$$

○ Data
— Least Squares Fit
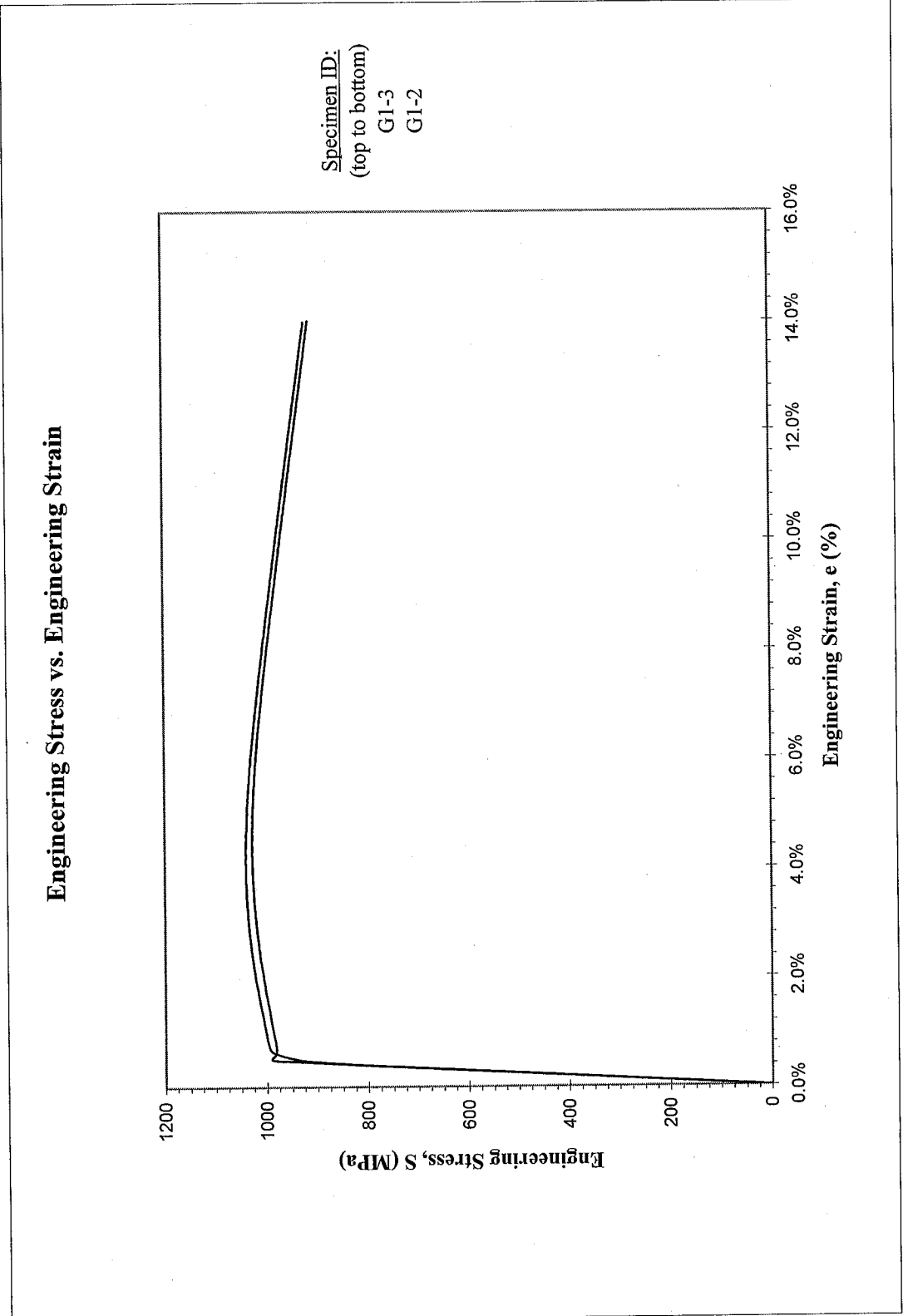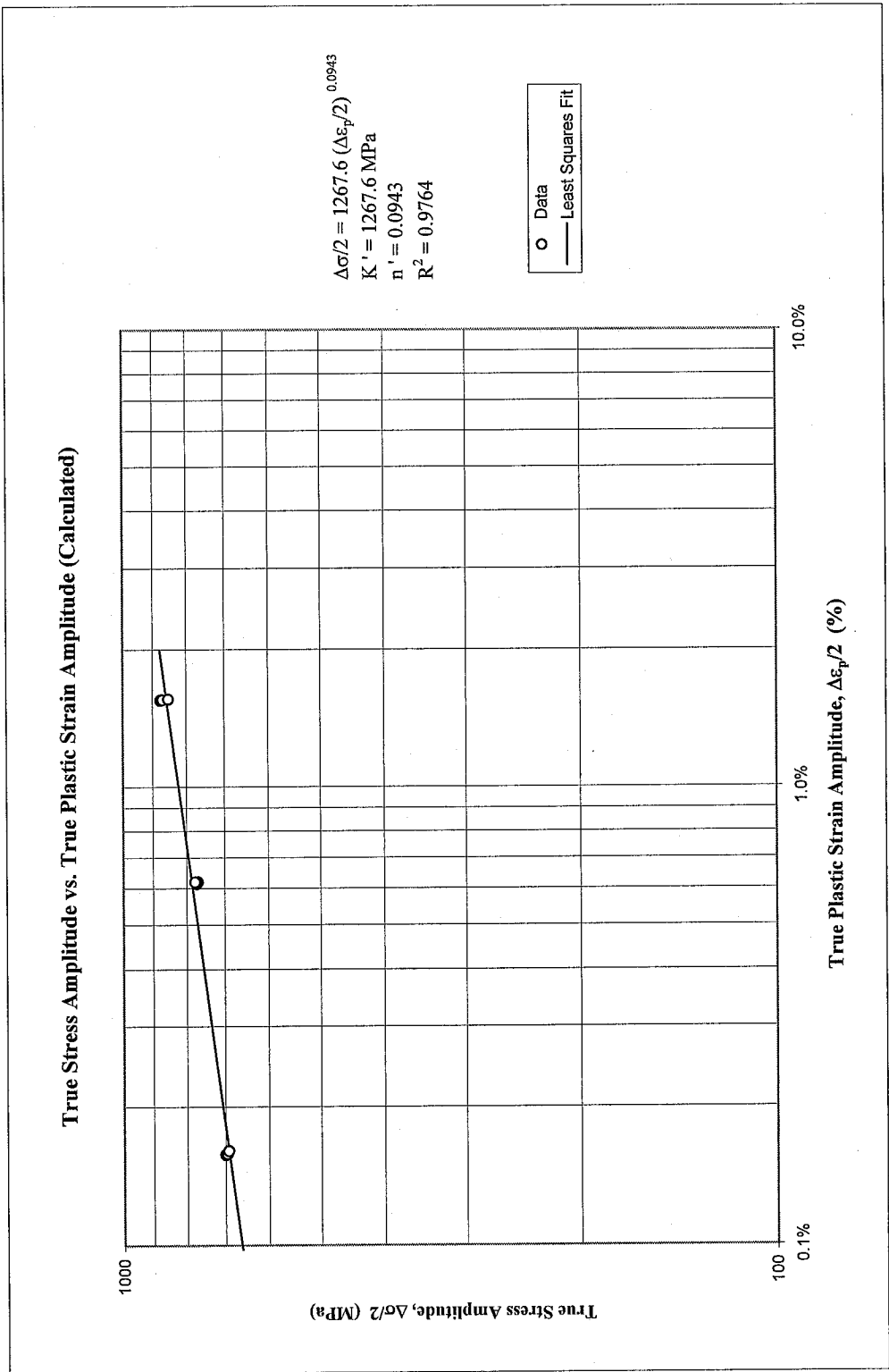

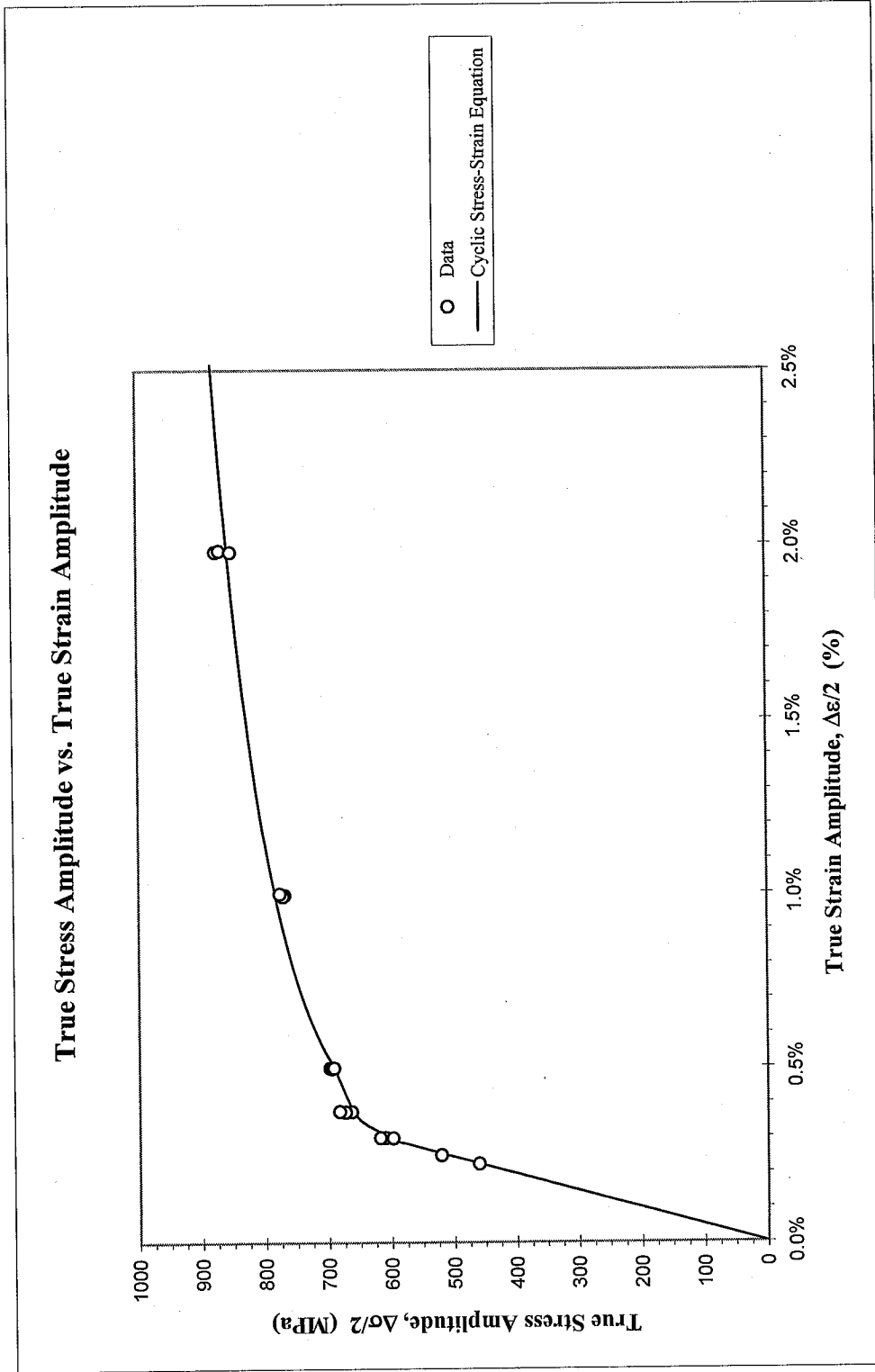Figure 6: True stress amplitude versus calculated true plastic strain amplitude

Figure 7: True stress amplitude versus true strain amplitude

22
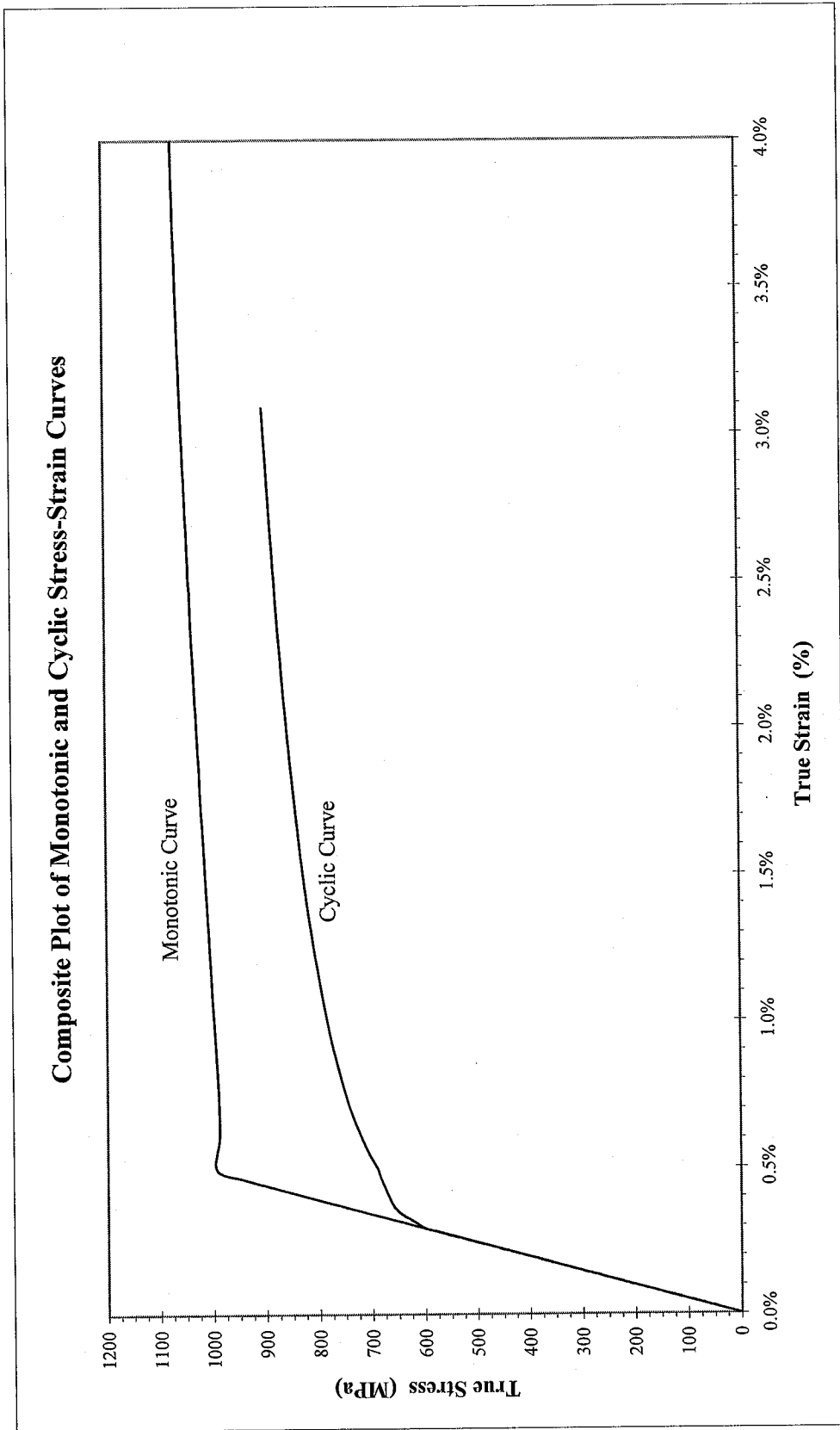
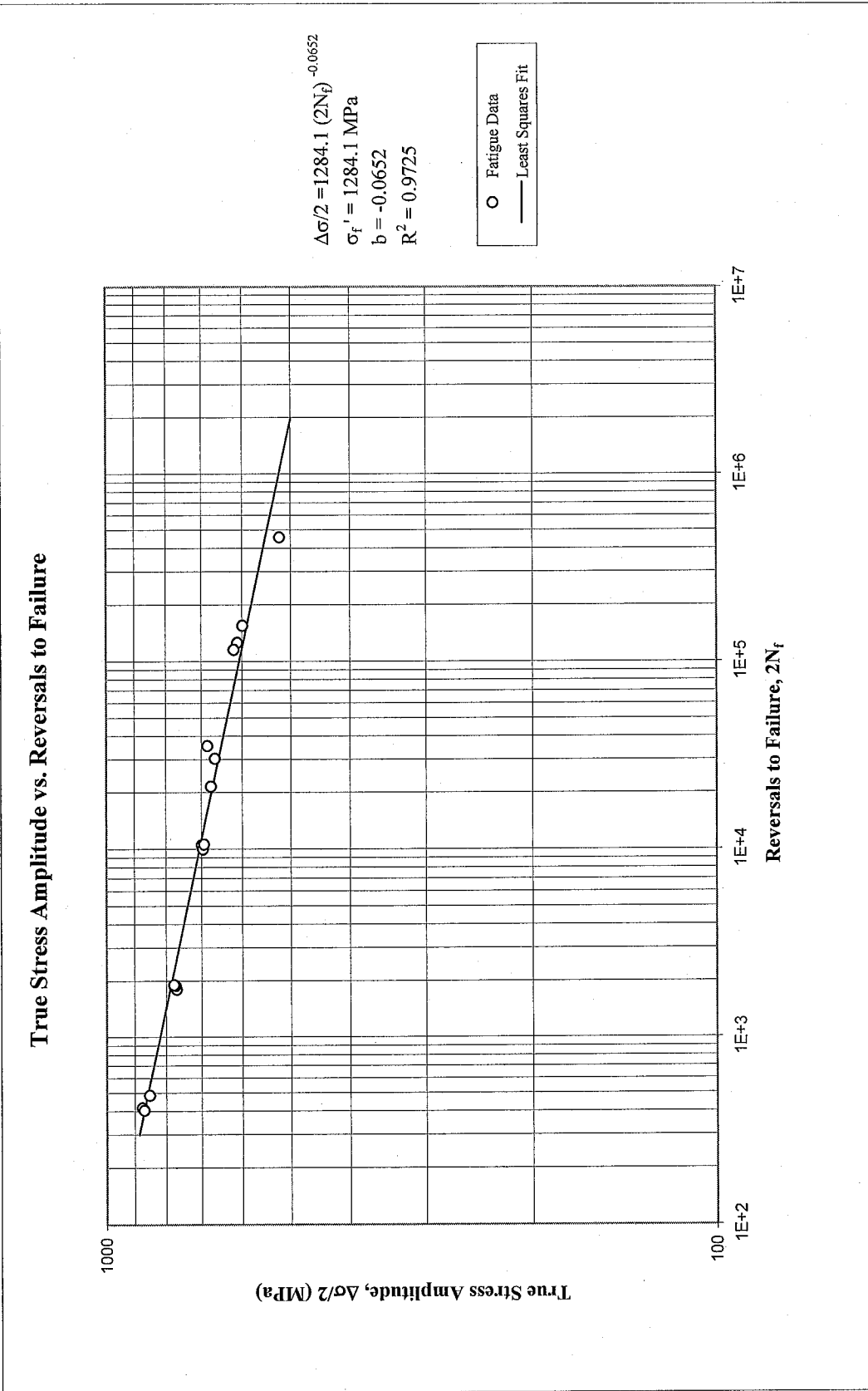Figure 8: Composite plot of cyclic and monotonic stress-strain curves

23

Figure 9: True stress amplitude versus reversals to failure

True Plastic Strain Amplitude (Calculated) vs. Reversals to Failure
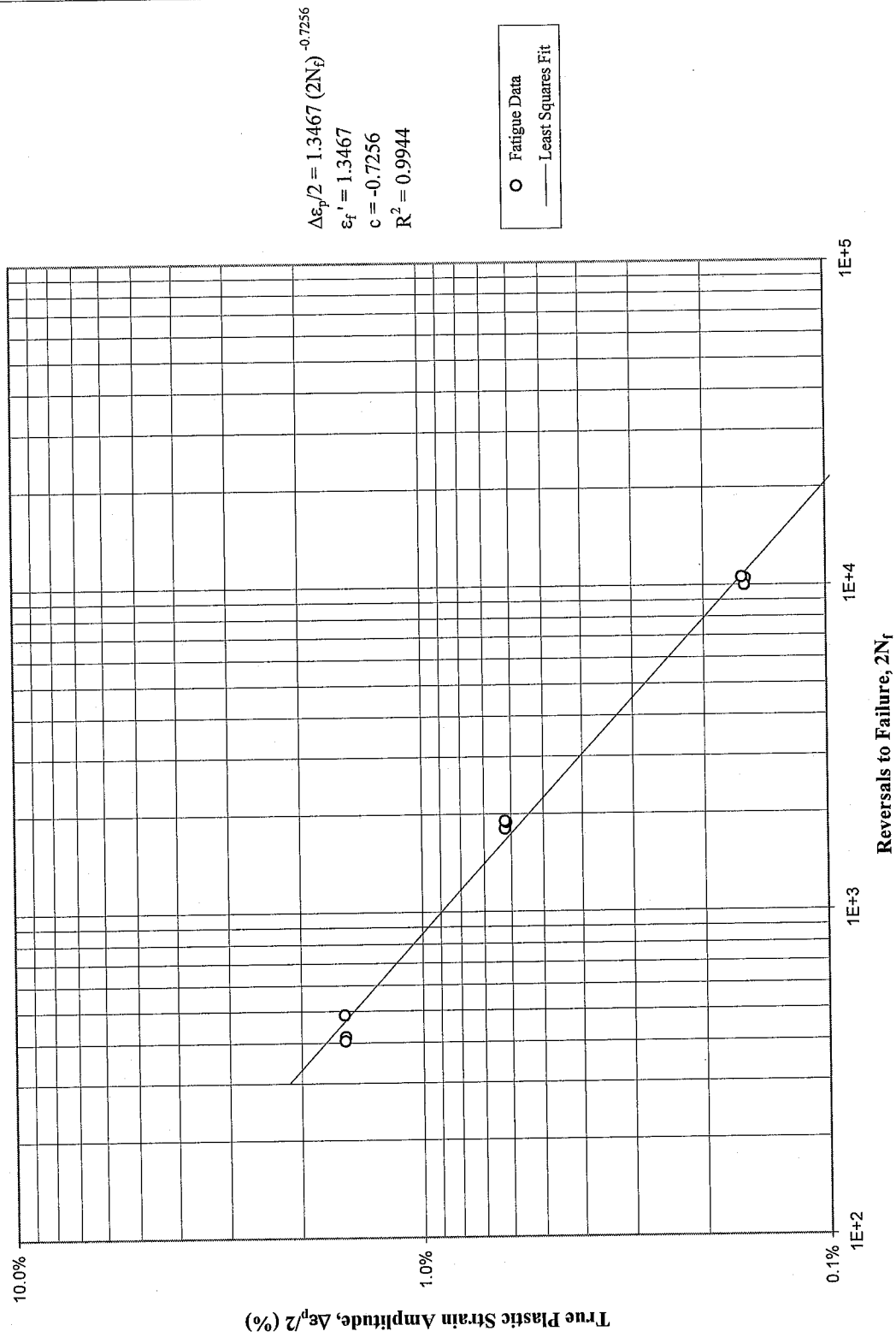

$$\Delta\varepsilon_p/2 = 1.3467 \, (2N_f)^{-0.7256}$$
$$\varepsilon_f' = 1.3467$$
$$c = -0.7256$$
$$R^2 = 0.9944$$

○ Fatigue Data
—— Least Squares Fit

Figure 10: Calculated true plastic strain amplitude versus reversals to failure
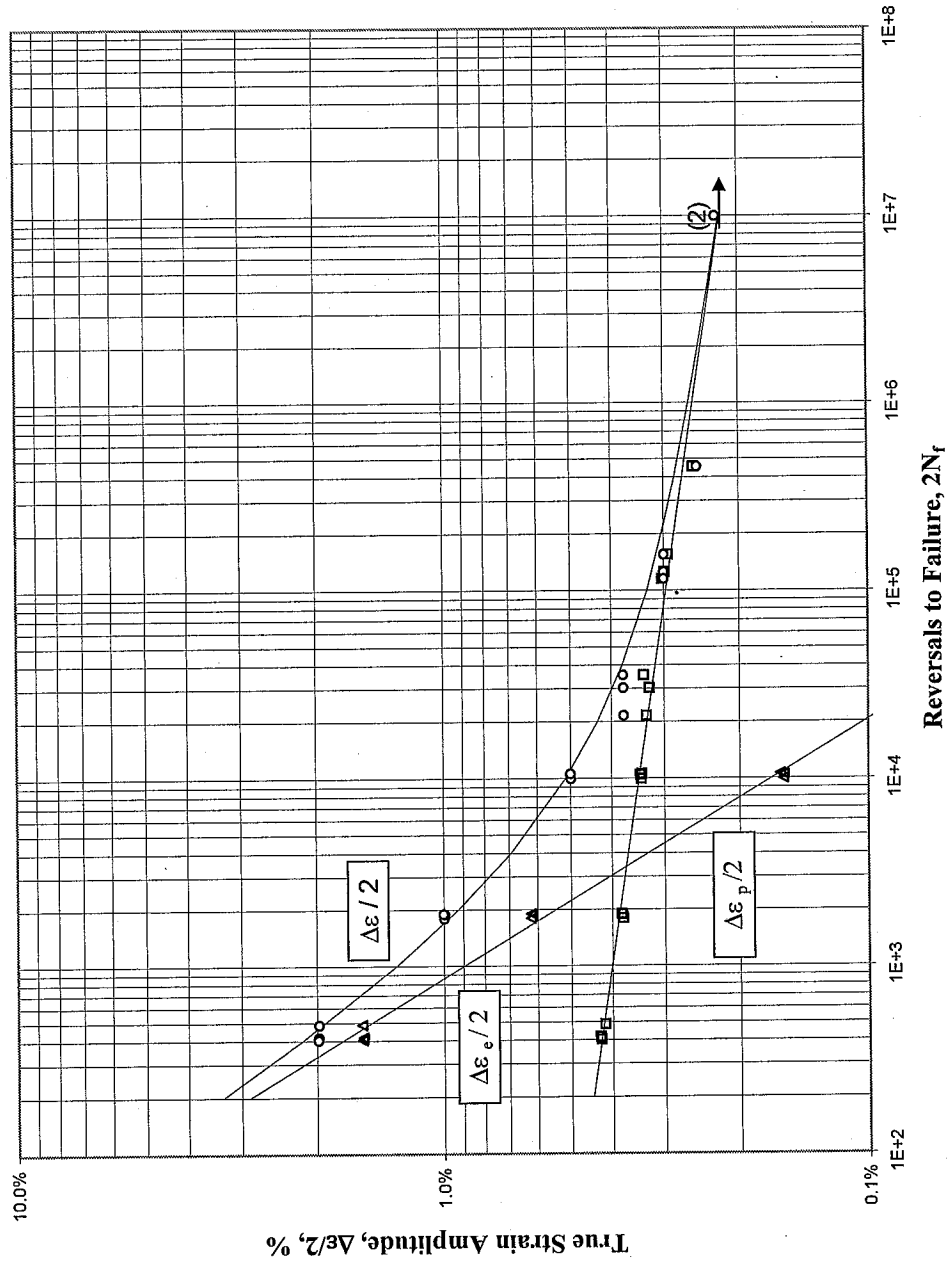
25

Figure 11: True strain amplitude versus reversals to failure

26

REFERENCES

[1] ASTM Standard E606-92, "Standard Practice for Strain-Controlled Fatigue Testing," Annual Book of ASTM Standards, Vol. 03.01, 1997, pp. 523-537.

[2] ASTM Standard E83-96, "Standard Practice for Verification and Classification of Extensometers," Annual Book of ASTM Standards, Vol. 03.01, 1997, pp. 198-206.

[3] ASTM Standard E1012-93a, "Standard Practice for Verification of Specimen Alignment Under Tensile Loading," Annual Book of ASTM Standards, Vol. 03.01, 1997, pp. 699-706.

[4] ASTM Standard E8-96a, "Standard Test Methods for Tension Testing of Metallic Materials," Annual Book of ASTM Standards, Vol. 03.01, 1997, pp. 56-76.

[5] ASTM Standard E112-96, "Standard Test Methods for Determining Average Grain Size," Annual Book of ASTM Standards, Vol. 03.01, 1997, pp. 227-249.

[6] ASTM Standard E45-97, "Standard Test Methods for Determining the Inclusion Content of Steel," Annual Book of ASTM Standards, Vol. 03.01, 1997, pp. 157-170.

[7] ASTM Standard E739-91, "Standard Practice for Statistical Analysis of Linear or Linearized Stress-Life (S-N) and Strain-Life (ε-N) Fatigue Data," Annual Book of ASTM Standards, Vol. 03.01, 1995, pp. 615-621.

[8] ASTM Standard E646-93, "Standard Test Method for Tensile Strain-Hardening Exponents (n-values) of Metallic Sheet Materials," Annual Book of ASTM Standards, Vol. 03.01, 1997, pp. 550-556.

[9] Bridgman, P. W., "Stress Distribution at the Neck of Tension Specimen," *Transactions of American Society for Metals*, Vol. 32, 1944, pp. 553-572.

APPENDIX

Table A.1: Summary of monotonic tensile test results

Specimen ID	D_o, mm (in.)	D_f mm (in.)	L_o, mm (in.)	L_f, mm (in.)	E, GPa (ksi)	YS (offset=0.2%), MPa (ksi)	UYS, MPa (ksi)	LYS, MPa (ksi)	YPE, %	S_u, MPa (ksi)	K, MPa (ksi)	n	%EL, %	%RA, %	R, mm (in.)	σ_f^*, MPa (ksi)	ε_f
G1-2	5.11 (0.20)	3.08 (0.12)	7.62 (0.30)	9.91 (0.39)	205.1 (29,747.7)	982.5 (142.5)	995.9 (144.4)	980.1 (142.2)	0.70%	1027.4 (149.0)	1,208.5 (175.3)	0.0379	30.0%	63.8%	1.63 (0.064)	858.8 (124.6)	101.5%
G1-3	5.05 (0.20)	3.05 (0.12)	7.62 (0.30)	9.86 (0.39)	203.8 (29,564.0)	995.6 (144.4)	NA	NA	NA	1040.8 (150.9)	1,217.5 (176.6)	0.0358	29.3%	63.6%	1.66 (0.065)	879.2 (127.5)	101.1%
Average values					204.5 (29,655.9)	989.0 (143.4)				1034.1 (150.0)	1213.0 (175.9)	0.0369	29.7%	63.7%	1.65 (0.065)	869.0 (126.0)	101.3%

* The values of true fracture strength are corrected for necking according to the Bridgman correction factor.

Table A.2: Summary of constant amplitude completely reversed fatigue test results

Specimen ID	Test control mode	Test freq., Hz	E, GPa (ksi)	At midlife ($N_{50\%}$)							$2N_{50\%}$, [a] reversals	$(2N_f)_{10\%}$, [b] reversals	$(2N_f)_{50\%}$, [c] reversals	Failure location [d]
				E', GPa (ksi)	$\Delta\varepsilon/2$, %	$\Delta\varepsilon_p/2$ (calculated), %	$\Delta\varepsilon_p/2$ (measured), %	$\Delta\sigma/2$, MPa (ksi)	σ_m, MPa (ksi)					
G1-7	strain	0.2	210.0 (30,460.0)	183.4 (26,603.1)	1.980%	1.553%	1.522%	874.2 (126.8)	-16.5 (-2.4)	188	410	418	IGL
G1-9	strain	0.2	207.0 (30,020.0)	180.9 (26,241.2)	1.983%	1.559%	1.517%	868.4 (125.9)	-14.2 (-2.1)	216	386	406	IGL
G1-11	strain	0.2	208.0 (30,170.0)	170.1 (24,676.2)	1.979%	1.563%	1.500%	850.6 (123.4)	-13.3 (-1.9)	256	472	488	IGL
G1-16	strain	0.5	203.1 (29,450.0)	178.9 (25,952.0)	0.996%	0.620%	0.570%	768.9 (111.5)	-6.5 (-0.9)	1,024	1,692	1,804	IGL
G1-8	strain	0.5	204.6 (29,680.0)	185.4 (26,895.4)	0.993%	0.616%	0.578%	771.7 (111.9)	-9.3 (-1.4)	1,024	1,726	1,890	IGL
G1-5	strain	0.5	208.3 (30,210.0)	184.2 (26,713.4)	1.000%	0.621%	0.581%	776.0 (112.5)	-10.0 (-1.5)	900	1,758	1,910	IGL
G1-1	strain	1.0	204.0 (29,590.0)	191.9 (27,825.5)	0.499%	0.158%	0.136%	698.0 (101.2)	-6.8 (-1.0)	5,716	10,126	10,488	IGL
G1-12	strain	1.0	205.2 (29,760.0)	191.8 (27,821.9)	0.498%	0.158%	0.138%	694.5 (100.7)	10.2 (1.5)	5,002	9,102	10,006	IGL
G1-10	strain	1.0	205.1 (29,750.0)	195.5 (28,352.4)	0.499%	0.161%	0.146%	691.7 (100.3)	-6.6 (-1.0)	5,300	9,584	10,596	IGL
G1-14	strain	1.5	202.5 (29,370.0)	198.4 (28,772.2)	0.374%	0.049%	0.038%	664.2 (96.3)	33.7 (4.9)	16,384	26,276	30,406	IGL
G1-13	strain	1.5	209.5 (30,390.0)	205.0 (29,738.2)	0.373%	0.043%	0.037%	673.8 (97.7)	8.4 (1.2)	16,384	21,008	21,598	IGL
G1-17	strain	1.5	204.7 (29,690.0)	200.2 (29,039.9)	0.375%	0.040%	0.034%	683.1 (99.1)	-38.4 (-5.6)	18,996	30,658	35,542	IGL
G1-4	strain / load	2.0 / 10.0	202.6 (29,390.0)	204.5 (29,652.5)	0.300%	0.001%	0.000%	609.8 (88.4) / 609.8 (88.4)	32.9 (4.8) / 0.0 (0.0)	34,498		126,230	IGL
G1-6	strain / load	2.0 / 10.0	201.1 (29,170.0)	200.3 (29,053.8)	0.299%	0.006%	0.000%	598.2 (86.8) / (598.2) (86.8)	12.5 (1.8) / 0.0 (0.0)	54,888		155,828	IGL
G1-15	strain / load	2.0 / 10.0	205.7 (29,830.0)	207.1 (30,043.3)	0.299%	0.000%	0.000%	618.4 (89.7) / 618.4 (89.7)	72.8 (10.6) / 0.0 (0.0)	3,708		116,008	IGL
G1-18	strain / load	2.0 / 25.0	208.8 (30,280.0)	209.3 (30,349.0)	0.250%	0.000%	0.000%	520.8 (75.5) / 520.8 (75.5)	-12.6 (-1.8) / 0.0 (0.0)	8,192		457,652	IGL
G1-19	strain / load	2.0 / 25.0	204.7 (29,690.0)	205.9 (29,867.3)	0.224%	0.000%	0.000%	460.4 (66.8) / 460.4 (66.8)	66.8 (9.7) / 0.0 (0.0)	11,068		>10,000,000	No Failure
G1-20	load	25.0			0.225%			460.4 (66.8)	0.0 (0.0)			>10,000,000	No Failure

[a] $N_{50\%}$ is defined as the midlife cycle (for run-out tests, data is taken from the stable cycle indicated).

[b] $(N_f)_{10\%}$ is defined as 10% load drop.

[c] $(N_f)_{50\%}$ is defined as 50% load drop.
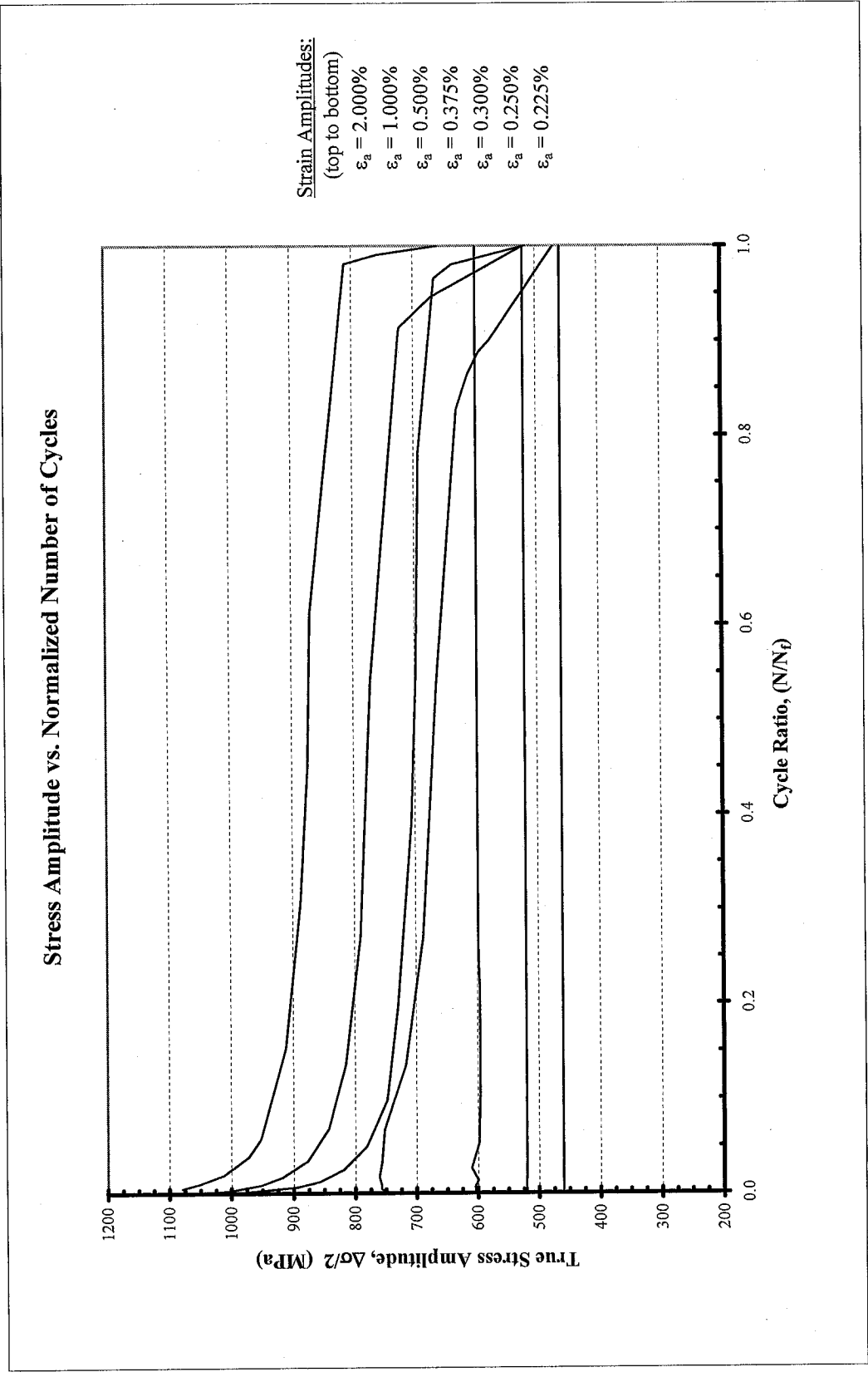
[d] IGL = inside gage length.

Figure A.1a: True stress amplitude versus normalized number of cycles
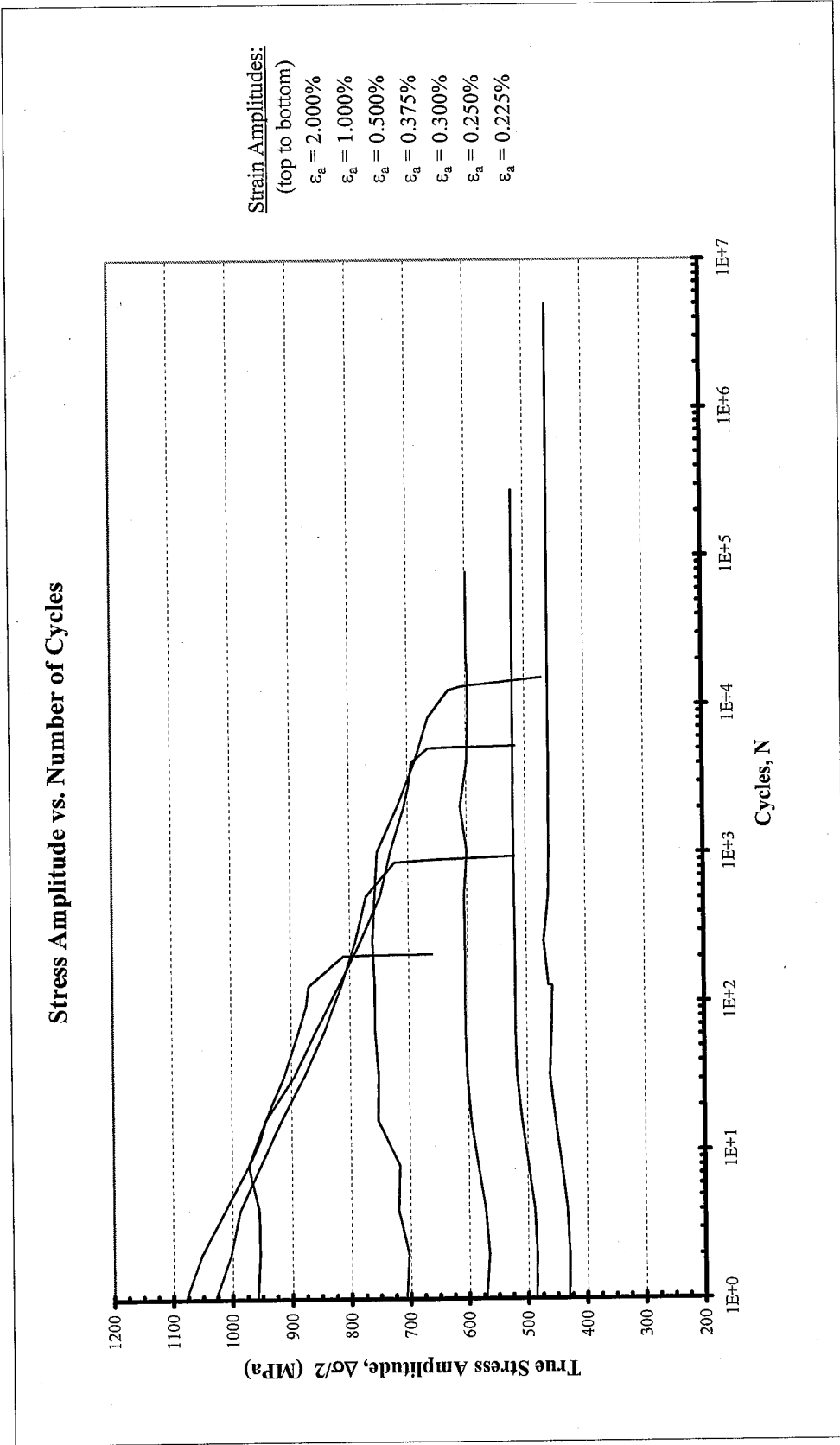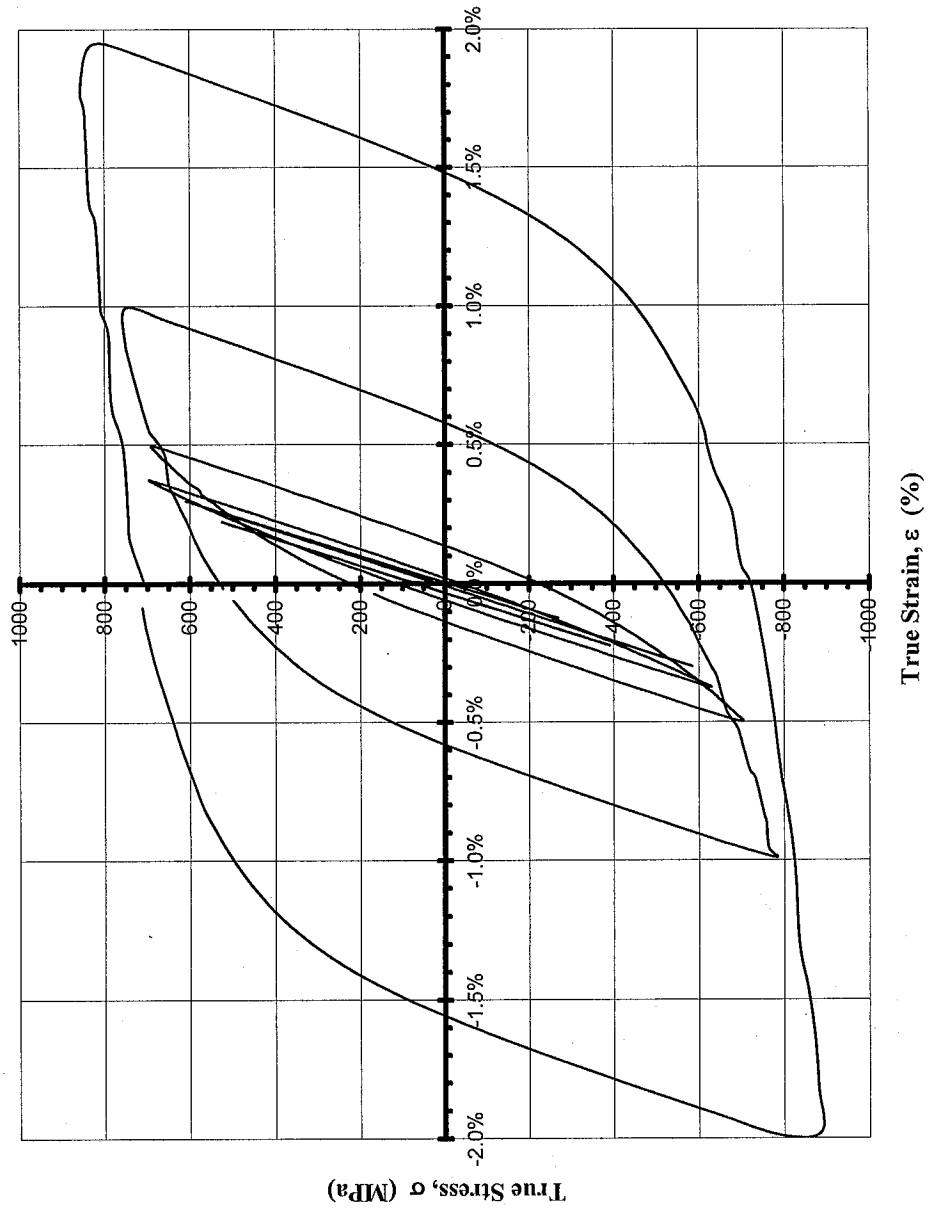
Figure A.1b: True stress amplitude versus number of cycles

Figure A.2: Composite plot of midlife hysteresis loops